

Performance of a Research Prototype Humanoid Robot *Bonten-Maru II* to Attain Human-Like Motions

HANAFIAH YUSSOF¹, MITSUHIRO YAMANO², YASUO NASU², MASAHIRO OHKA¹

¹Graduate School of Information Science, Nagoya University
Furo-cho Chikusa-ku Nagoya Aichi 466-0815

²Department of Mechanical Systems Engineering, Faculty of Engineering, Yamagata University
Jonan 4-3-16 Yonezawa Yamagata 992-8510

JAPAN

hanafiah@nuem.nagoya-u.ac.jp http://ns1.ohka.cs.is.nagoya-u.ac.jp/ohka_lab2/index_eng.html

Abstract: - This report presents development of basic human-like motions using a research prototype 21-dof humanoid robot called *Bonten-Maru II*. The aim is to create suitable motion trajectories towards application of humanoid robots in real environments. Kinematical analysis of 3-dof arm and 6-dof leg were presented to generate trajectory in the robot's arms and legs. To realize human-like motions, we proposed navigation method based on contact interaction for humanoid robot to recognize its surrounding by grasping object surface and then correcting its locomotion direction. We also proposed methods to avoid high and low obstacles. Finally, we present crawling motions which can be applied during operation in emergency sites. The experimental results utilizing *Bonten-Maru II* revealed good performance of the robot when performing human-like motions in the proposed navigation method, obstacle avoidance, and crawling motions.

Key-Words: - Humanoid robot, human-like motions, trajectory generation, kinematics, contact-based navigation, obstacle avoidance, crawling motion

1 Introduction

Research in humanoid robotics is currently shifting from locomotion and stability issues to interaction between humans and robots. These motivations are derived from the intention to develop intelligent and human-friendly machine to replace human in dangerous sites, to assist the elderly and the disabled, to entertain children and to communicate in a natural language. This will provide humans with more safety, freedom and time.

Humanoid robots are the type of robot that practically suitable to coexist with human in built-for-human environment because of its anthropomorphism, human friendly design and locomotion ability [1][2]. Humanoid robot is different compare to other types of robots because the physical structure is designed to mimic as much as human's physical structure. Humanoid's shape shares many basic physical characteristics with actual humans, and for this reason, they are expected to coexist and collaborate with humans in environments where humans work and live. They may also be substituted for humans in hazardous environments or at disaster sites. These demands make it imperative for humanoid robots to attain many sophisticated motions such as walking, climbing stairs, avoiding obstacles, crawling, etc.

It is apparent that to work with humans, humanoid robots must be able to recognize and perform human-like motion. In the past decade, we have seen enthusiastic efforts by robot researchers to develop anthropomorphic humanoid robots, ones that can think intelligently and mimic human action [3-6]. The most successful introduction of humanoid robots nowadays probably goes to *Asimo*, *Qrio* and *HRP-2*. In our research laboratory, we have developed a research prototype 21-dof humanoid robot called *Bonten-Maru II*. *Bonten-Maru II* is a low-cost research prototype humanoid robot and is one of few research prototype humanoid robots in the world which can be utilized in various aspects of studies. It is our goal that the works done in the *Bonten-Maru II* projects will give some impact on further research in the humanoid robotics.

In this report, we present experimental results of humanoid robot *Bonten-Maru II* to attain human-like motion with the aim to operate in built-for-human environment. Firstly, we present method to solve kinematics problems in trajectory generation of the robot arms and legs. Second we introduced navigation strategy applying contact interaction where humanoid robot touch and grasp object using its arms and correcting its locomotion directions. Finally we present motions of avoiding low and high obstacles, and crawling.

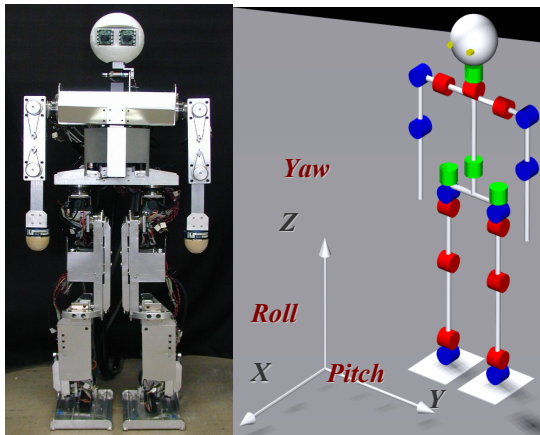


Fig. 1. Humanoid robot *Bonten-Maru II* and configuration of dofs.

2 Structure and Specifications of Humanoid Robot *Bonten-Maru II*

In this research we utilized a 21-dof humanoid robot *Bonten-Maru II* [7]. Appearance diagram of the humanoid robot *Bonten-Maru II* is shown in Fig. 1. This figure also displays configuration of dofs in the humanoid robot's body. This robot is 1.25 [m] tall and weight 31.5 [kg], which similar to an eight or nine year old child. The *Bonten-Maru II* is a research prototype humanoid robot, and such has undergone some refinement as different research direction is considered. During the design process, some predefined degree of stiffness, accuracy, repeatability, and other design factor have been taken into consideration.

The *Bonten-Maru II* was designed to mimic as much as human characteristic, especially for contribution of its joints. *Bonten-Maru II* is consists of total of 21-dofs: six for each leg, three for each arm, one for the waist, and two for the head. The high numbers of dofs provide the ability to realize complex motions. Furthermore, the configuration of joints that closely resemble those of humans provides the advantages for the humanoid robot to attain human-like motion. Each joint feature a relatively wide range of rotation angles, shown in Table 1, particularly for the hip yaw of both legs, which permits the legs to rotate through wide angles when correcting the robot's orientation and avoiding obstacles. The specification of each joint rotation range is considered factors such as correlation with human's joint rotation range, manipulability of humanoid's manipulator, and safety during performing motions [8]. Every joint is driven by DC servomotor with a rotary encoder and harmonic drive reduction system, and PC with Linux (CPU: Celeron 2.4 GHz) is utilized for control. The sampling frequency is 200 Hz.

Table 1. Joint rotation range of *Bonten-Maru II*.

Axis	<i>Bonten-Maru II</i> (deg)	Human (deg)
Neck (roll and pitch)	-90 ~ 90	-90 ~ 90
Shoulder (pitch) right & left	-180 ~ 120	-180 ~ 120
Shoulder (roll) right/left	-135 ~ 30/-30 ~ 135	-135 ~ 30/-30 ~ 135
Elbow (roll) right/left	0 ~ 135/0 ~ -135	0 ~ 135/0 ~ -135
Waist (yaw)	-90 ~ 90	-45 ~ 45
Hip (yaw) right/left	-90 ~ 60/-60 ~ 90	-90 ~ 60/-60 ~ 90
Hip (roll) right/left	-90 ~ 22/-22 ~ 90	-60 ~ 45/-45 ~ 60
Hip (pitch) right & left	-130 ~ 45	-130 ~ 45
Knee (pitch) right & left	-20 ~ 150	0 ~ 150
Ankle (pitch) right & left	-90 ~ 60	-30 ~ 90
Ankle (roll) right/left	-20 ~ 90/-90 ~ 20	-20 ~ 30/-30 ~ 20

The power is supplied to each joint by timing belt and harmonic drive reduction system. Gear number at the DC servomotor side is 60; while at the harmonic drive side is 16. Therefore, it makes reduction ratio at the harmonic side to be 1:100, while overall reduction ratio is 1:333. The motor driver, the PC and the power supply are placed outside of the robot. *Bonten-Maru II* is equipped with a force sensor in both arms. As for the legs, there are four pressure sensors under each foot: two under the toe area and two under the heel. These provide a good indication that both legs are in contact with the ground. The head part is equipped with two color CCD cameras (542 x 492 pixels).

3 Trajectory Generation

Trajectory generation to perform motions for biped locomotion robots is normally defined by solving forward and inverse kinematics problems [9]. Calculation to solve kinematics problems for robotic joints is a complicated and time-consuming study, especially when it involves a complex joint structure. In a forward kinematics problem, where the joint variable is given, it is easy to determine the end-effector's position and orientation. An inverse kinematics problem, however, in which each joint variable is determined by using end-effector position and orientation data, does not guarantee a closed-form solution. Traditionally three methods are used to solve an inverse kinematics problem: geometric, iterative, and algebraic [10]. However, the more complex the manipulator's joint structure, the more complicated and time-consuming these methods become.

In this paper, we propose and implement a simplified approach to solving inverse kinematics problems by classifying the robot's joints into several groups of joint coordinate frames at the robot's manipulator [11]. To describe translation and rotational relationship between adjacent joint links, we employ a matrix method proposed by Denavit-Hartenberg [12], which systematically establishes a coordinate system for each link of an articulated chain in the robot body.

3.1 Kinematical Solutions for 3-dof Arm

The humanoid robot *Bonten-Maru II* has three dofs on each arm: two dofs (pitch and roll) at the shoulder joint and one dof (roll) at the elbow joint. Figure 2 shows the arm structure and configuration of joints and links. The coordinate orientation follows the right-hand law, and a reference coordinate is fixed at the intersection point of two joints at the shoulder. Figure 3 displays a model of the robot arm describing the configurations and orientation of each joint coordinates. To avoid confusion, only the x and z -axes appear in the figure. The arm's structure is divided into five sets of joint-coordinates frames as listed below:

- Σ_0 : Reference coordinate.
- Σ_1 : Shoulder joint pitch coordinate.
- Σ_2 : Shoulder joint roll coordinate.
- Σ_3 : Elbow joint roll coordinate.
- Σ_h : End-effector coordinate.

Consequently, corresponding link parameters of the arm can be defined as shown in Table 2. From the Denavit-Hartenberg convention mentioned above, definitions of the homogeneous transform matrix of the link parameters can be described as follows:

$${}^0_h \mathbf{T} = \text{Rot}(z, \theta) \text{Trans}(0, 0, d) \text{Trans}(l, 0, 0) \text{Rot}(x, \alpha). \quad (1)$$

Here, variable factor θ_i is the joint angle between the x_{i-1} and the x_i axes measured about the z_i axis; d_i is the distance from the x_{i-1} axis to the x_i axis measured along the z_i axis; α_i is the angle between the z_i axis to the z_{i-1} axis measured about the x_{i-1} axis, and l_i is the distance from the z_i axis to the z_{i-1} axis measured along the x_{i-1} axis. Here, link length for the upper and lower arm is described as l_1 and l_2 , respectively. The following is used to obtain the forward kinematics solution for the robot arm:

$${}^0_h \mathbf{T} = {}^0_1 \mathbf{T} {}^1_2 \mathbf{T} {}^2_3 \mathbf{T} {}^3_h \mathbf{T}$$

$$= \begin{bmatrix} s_1 c_{23} & -s_1 s_{23} & c_1 & s_1(l_1 c_2 + l_2 c_{23}) \\ s_{23} & c_{23} & 0 & l_1 s_2 + l_2 s_{23} \\ -c_1 c_{23} & c_1 s_{23} & s_1 & -c_1(l_1 c_2 + l_2 c_{23}) \\ 0 & 0 & 0 & 1 \end{bmatrix}. \quad (2)$$

Table 2. Link parameters of the robot arm.

Link	$\theta_{i\text{arm}}$	d	α	l
0	$\theta_{1\text{arm}} - 90^\circ$	0	90°	0
1	$\theta_{2\text{arm}}$	0	-90°	0
2	$\theta_{3\text{arm}}$	0	0	l_1
3	0	0	0	l_2

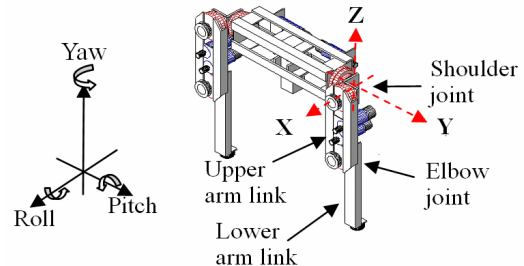


Fig. 2. Arm structure of *Bonten-Maru II*.

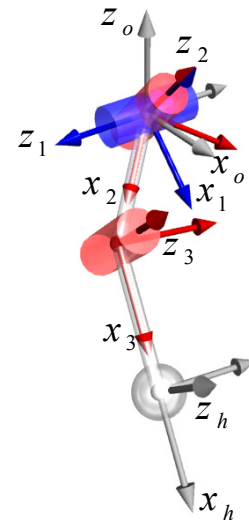


Fig. 3. Configurations of joint coordinates at the robot arm.

The end-effector's orientation with respect to the reference coordinate (${}^0_h \mathbf{R}$) is shown in (3), while the position of the end-effector (${}^0_h \mathbf{P}_h$) is shown in (4). The position of the end-effector in regard to global axes P_x , P_y and P_z can be define by (5). Here, s_i and c_i are respective abbreviations of $\sin \theta_i$ and $\cos \theta_i$, where ($i=1, 2, \dots, n$) and n is equal to quantity of dof.

$${}^0_h \mathbf{R}_{\text{arm}} = \begin{bmatrix} s_1 c_{23} & -s_1 s_{23} & c_1 \\ s_{23} & c_{23} & 0 \\ -c_1 c_{23} & c_1 s_{23} & s_1 \end{bmatrix} \quad (3)$$

$${}^0_h \mathbf{P}_{\text{arm}} = \begin{bmatrix} s_1(l_1 c_2 + l_2 c_{23}) \\ l_1 s_2 + l_2 s_{23} \\ -c_1(l_1 c_2 + l_2 c_{23}) \end{bmatrix} \quad (4)$$

$$\left. \begin{aligned} P_{x\text{arm}} &= s_1(l_1 c_2 + l_2 c_{23}) \\ P_{y\text{arm}} &= l_1 s_2 + l_2 s_{23} \\ P_{z\text{arm}} &= -c_1(l_1 c_2 + l_2 c_{23}) \end{aligned} \right\} \quad (5)$$

As understood from (3) and (4), a forward kinematics equation can be used to compute the Cartesian coordinates of the robot arm when the joint angles are known. However, in real-time applications it is more practical to provide the end-effector's position and orientation data to the robot's control system than to define each joint angle that involved complicated calculations. Therefore, inverse kinematics solutions are more favourable for generating the trajectory of the humanoid robot manipulator. To define joint angles θ_{1arm} , θ_{2arm} , θ_{3arm} in an inverse kinematics problem, at first each position element in (5) is multiplied and added to each other according to (6), which can also be arranged as (7). Thus, θ_{3arm} is defined in (8).

$$P_{xarm}^2 + P_{yarm}^2 + P_{zarm}^2 = l_1^2 + l_2^2 + 2l_1l_2c_3 \quad (6)$$

$$c_3 = \frac{P_{xarm}^2 + P_{yarm}^2 + P_{zarm}^2 - (l_1^2 + l_2^2)}{2l_1l_2} = C \quad (7)$$

$$\theta_{3arm} = \text{atan2}\left(\pm\sqrt{1-C^2}, C\right) \quad (8)$$

Referring to the rotation direction of θ_{3arm} , if $\sin\theta_{3arm}$ is a positive value, it describes the inverse kinematics for the right arm, while if it is a negative value it described the left arm. Consequently, θ_{3arm} is used to define θ_{2arm} , as shown in (9) ~ (13), where newly polar coordinates are defined in (11). Consequently, θ_{1arm} can be defined as in (14).

$$k_1 = l_1 + l_2c_3, \quad k_2 = -l_2s_3 \quad (9)$$

$$p_{xz} = k_1c_2 + k_2s_2, \quad p_y = k_2c_2 - k_1s_2 \quad (10)$$

$$\phi = \text{atan2}(k_1, k_2) \quad (11)$$

$$\phi + \theta_{2arm} = \text{atan2}\left(\frac{p_{xz}}{r}, \frac{p_y}{r}\right) \quad (12)$$

$$= \text{atan2}(p_{xz}, p_y)$$

$$\theta_{2arm} = \text{atan2}(p_{xz}, p_y) - \text{atan2}(k_1, k_2) \quad (13)$$

$$\theta_{1arm} = \text{atan2}\left(\frac{p_x}{p_{xz}}, \frac{p_z}{p_{xz}}\right) \quad (14)$$

$$= \text{atan2}(p_x, p_z)$$

3.2 Kinematical Solutions for 6-dof Leg

Each of the legs has six dofs: three dofs (yaw, roll and pitch) at the hip joint, one dof (pitch) at the knee joint and two dofs (pitch and roll) at the ankle joint. In this research, we solve only inverse kinematics calculations for the robot leg. Figure 4 shows the structure and configuration of joints and links in the robot's leg. A reference coordinate is taken at the

intersection point of the 3-dof hip joint. In solving calculations of inverse kinematics for the leg, just as for arm, the joint coordinates are divided into eight separate coordinate frames as listed bellow.

- Σ_0 : Reference coordinate.
- Σ_1 : Hip yaw coordinate.
- Σ_2 : Hip roll coordinate.
- Σ_3 : Hip pitch coordinate.
- Σ_4 : Knee pitch coordinate.
- Σ_5 : Ankle pitch coordinate.
- Σ_6 : Ankle roll coordinate.
- Σ_h : Foot bottom-center coordinate.

Table 3. Link parameters of the leg.

Link	θ_{ileg}	d	α	l
0	$\theta_{1leg} + 90^\circ$	0	0	0
1	$\theta_{2leg} - 90^\circ$	0	90°	0
2	θ_{3leg}	0	90°	0
3	θ_{4leg}	0	0	l_1
4	θ_{5leg}	0	0	l_2
5	θ_{6leg}	0	-90°	0
6	0	0	0	l_3

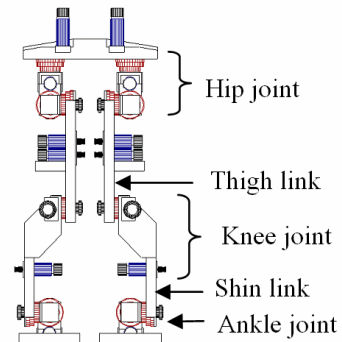


Fig. 4. Leg structure of Bonten-Maru II.

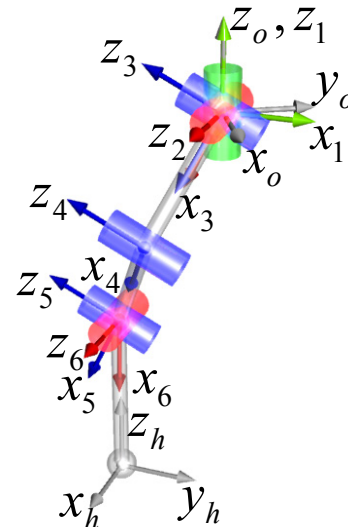


Fig. 5. Configurations of joint coordinates at the robot leg.

Figure 5 shows a model of the robot leg that indicates the configurations and orientation of each set of joint coordinates. Here, link length for the thigh is l_1 , while for the shin it is l_2 . The same convention applies for the arm link parameter mentioned earlier. Link parameters for the leg are defined in Table 3.

Referring to Fig. 5, the transformation matrix at the bottom of the foot (${}^6_h \mathbf{T}$) is an independent link parameter because the coordinate direction is changeable. Here, to simplify the calculations, the ankle joint is positioned so that the bottom of the foot settles on the floor surface. The leg's orientation is fixed from the reference coordinate so that the third row of the rotation matrix at the leg's end becomes like (15).

$$P_{zleg} = [0 \ 0 \ 1]^T \quad (15)$$

Furthermore, the leg's links are classified into three groups to short-cut the calculations, where each group of links is calculated separately as follows:

- i) From link 0 to link 1 (Reference coordinate to coordinate joint number 1).
- ii) From link 1 to link 4 (Coordinate joint number 2 to coordinate joint number 4).
- iii) From link 4 to link 6 (Coordinate joint number 5 to coordinate at the bottom of the foot).

Basically, i) is to control leg rotation at the z -axis, ii) is to define the leg position, while iii) is to decide the leg's end-point orientation. A coordinate transformation matrix can be arranged as below.

$${}^0_h \mathbf{T} = {}^0_1 \mathbf{T} {}^1_4 \mathbf{T} {}^4_h \mathbf{T} = ({}^0_h \mathbf{T}) ({}^1_2 \mathbf{T} {}^2_3 \mathbf{T} {}^3_4 \mathbf{T}) ({}^4_5 \mathbf{T} {}^5_6 \mathbf{T} {}^6_h \mathbf{T}) \quad (16)$$

Here, the coordinate transformation matrices for ${}^1_4 \mathbf{T}$ and ${}^4_h \mathbf{T}$ can be defined as (17) and (18), respectively.

$${}^1_4 \mathbf{T} = {}^1_2 \mathbf{T} {}^2_3 \mathbf{T} {}^3_4 \mathbf{T} = \begin{bmatrix} s_2 c_{34} & -s_2 s_{34} & -c_2 & l_1 s_2 c_3 \\ -s_{34} & -c_{34} & 0 & -l_1 s_3 \\ -c_2 c_{34} & c_2 s_{34} & -s_2 & -l_1 c_2 c_3 \\ 0 & 0 & 0 & 1 \end{bmatrix} \quad (17)$$

$${}^4_h \mathbf{T} = {}^4_5 \mathbf{T} {}^5_6 \mathbf{T} {}^6_h \mathbf{T} = \begin{bmatrix} c_5 c_6 & -c_5 s_6 & -s_5 & l_2 + l_3 c_5 c_6 \\ s_5 c_6 & -s_5 s_6 & c_5 & l_3 s_5 c_6 \\ -s_6 & -c_6 & 0 & -l_3 s_6 \\ 0 & 0 & 0 & 1 \end{bmatrix} \quad (18)$$

The coordinate transformation matrix for ${}^0_h \mathbf{T}$, which describes the leg's end-point position and orientation, can be shown with the following equation.

$${}^0_h \mathbf{T} = \begin{bmatrix} r_{11} & r_{12} & r_{13} & P_x \\ r_{21} & r_{22} & r_{23} & P_y \\ r_{31} & r_{32} & r_{33} & P_z \\ 0 & 0 & 0 & 1 \end{bmatrix} \quad (19)$$

From equation (15), the following conditions were satisfied.

$$r_{13} = r_{23} = r_{31} = r_{32} = 0, \quad r_{33} = 1 \quad (20)$$

Hence, joint rotation angles $\theta_{1leg} \sim \theta_{6leg}$ can be defined by applying the above conditions.

First, considering i), in order to provide rotation at the z -axis, only the hip joint needs to rotate in the yaw direction, specifically by defining θ_{1leg} . As mentioned earlier, the bottom of the foot settles on the floor surface; therefore, the rotation matrix for the leg's end-point measured from the reference coordinate can be defined by the following equation.

$${}^0_h \mathbf{R} = \text{Rot}(z, \theta_{1leg}) = \begin{bmatrix} c\theta_{1leg} & -s\theta_{1leg} & 0 \\ s\theta_{1leg} & c\theta_{1leg} & 0 \\ 0 & 0 & 1 \end{bmatrix} = \begin{bmatrix} r_{11} & r_{12} & 0 \\ r_{21} & r_{22} & 0 \\ 0 & 0 & 1 \end{bmatrix} \quad (21)$$

Here, θ_{1leg} can be defined as below.

$$\theta_{1leg} = \text{atan2}(r_{21}, r_{22}) \quad (22)$$

Next, considering ii), from the obtained result of θ_{1leg} , ${}^0_h \mathbf{T}$ is defined in (23).

$${}^0_h \mathbf{T} = \begin{bmatrix} -s_l & -c_l & 0 & P_{xleg} \\ c_l & -s_l & 0 & P_{yleg} \\ 0 & 0 & 1 & P_{zleg} \\ 0 & 0 & 0 & 1 \end{bmatrix} \quad (23)$$

Here, from constrain orientation of the leg's end point, the position vector of joint 5 is defined as follows in (24), and its relative connection with the matrix is defined in (25). Next, equation (26) is defined relatively.

$${}^0 \mathbf{P}_5 = {}^0_4 \mathbf{T} {}^4 \mathbf{P}_5 = \begin{bmatrix} P_{xleg} & P_{yleg} & P_{zleg} - l_3 \end{bmatrix}^T, \quad (24)$$

$${}^1_4 \mathbf{T} {}^4 \hat{\mathbf{P}}_5 = {}^1_4 \mathbf{T}^{-1} {}^0 \hat{\mathbf{P}}_5 \quad (25)$$

$$\begin{bmatrix} s_2 c_{34} & -s_2 s_{34} & -c_2 & l_1 s_2 c_3 \\ -s_{34} & -c_{34} & 0 & -l_1 s_3 \\ -c_2 c_{34} & c_2 s_{34} & -s_2 & -l_1 c_2 c_3 \\ 0 & 0 & 0 & 1 \end{bmatrix} \begin{bmatrix} l_2 \\ 0 \\ 0 \\ 1 \end{bmatrix} \quad (26)$$

$$= \begin{bmatrix} -s_l & c_l & 0 & 0 \\ -c_l & -s_l & 0 & 0 \\ 0 & 0 & 1 & 0 \\ 0 & 0 & 0 & 1 \end{bmatrix} \begin{bmatrix} p_x \\ p_y \\ p_z - l_3 \\ 1 \end{bmatrix}$$

$$\text{Therefore, } \begin{bmatrix} \hat{P}_{xleg} \\ \hat{P}_{yleg} \\ \hat{P}_{zleg} \end{bmatrix} = \begin{bmatrix} s_2(l_1 c_3 + l_2 c_{34}) \\ -(l_1 c_3 + l_2 s_{34}) \\ -c_2(l_1 c_3 + l_2 c_{34}) \end{bmatrix}. \quad (27)$$

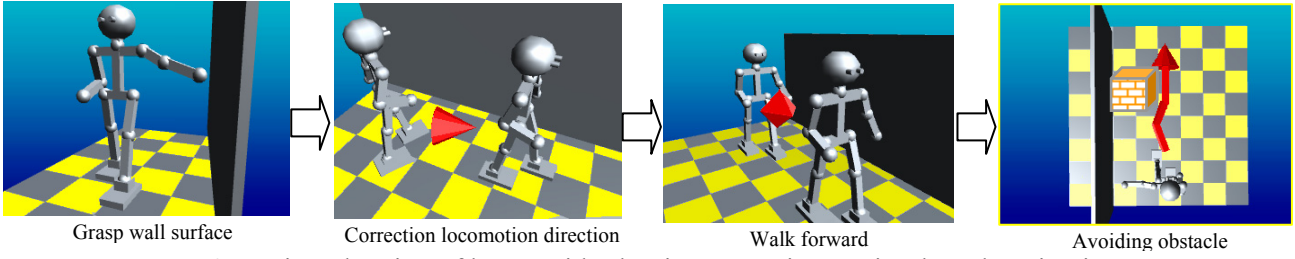


Fig.6. Motion planning of humanoid robot in contact interaction-based navigation.

To define joint angles θ_{2leg} , θ_{3leg} , θ_{4leg} , equation (27) is used, and it is similar to the calculation for solving inverse kinematics using equation (5) for the arm. Therefore, the rotation angles are defined as the following equations:

$$\theta_{4leg} = \text{atan2}\left(\pm\sqrt{I-C^2}, C\right) \quad (28)$$

$$\theta_{3leg} = \text{atan2}(\hat{p}_{xzleg}, \hat{p}_{yleg}) + \text{atan2}(k_1, k_2) \quad (29)$$

$$\theta_{2leg} = \text{atan2}(\hat{p}_{xleg}, \hat{p}_{zleg}) \quad (30)$$

Eventually, C , \hat{p}_{xzleg} , k_1 , k_2 are defined as follows.

$$C = \frac{\hat{p}_{xleg}^2 + \hat{p}_{yleg}^2 + \hat{p}_{zleg}^2 - (l_1^2 + l_2^2)}{2l_1l_2} \quad (31)$$

$$\hat{p}_{xzleg} = \sqrt{\hat{p}_{xleg}^2 + \hat{p}_{zleg}^2} \quad (32)$$

$$k_1 = l_1 + l_2c_4, \quad k_2 = -l_2s_4 \quad (33)$$

Finally, considering iii), joint angles θ_{5leg} and θ_{6leg} are defined geometrically as following equations.

$$\theta_{5leg} = -\theta_{3leg} - \theta_{4leg} \quad (34)$$

$$\theta_{6leg} = -\theta_{2leg} \quad (35)$$

4 Motions of Contact Interaction-Based Navigation

The application of humanoid robots in the same workspace with humans inevitably results in direct physical-contact interaction. Besides vision based interaction which obviously provides better information about the environment, the ability of the robot to operate in darkness is inevitably important. Eventually, contact interaction-based method is practically suitable for application in hazardous sites, dark areas or during operation in confined spaces. This is because the non-contact interaction method which usually used cameras, radar sensors, etc. are easily interrupted by environment factors such as darkness, smoke, dusts, etc. Meanwhile, contact interaction offers better options for humanoid robots to accurately gauge the structure of their environment [13]. As blind people convincingly demonstrate, physical contact interaction alone can support extremely sophisticated motions.

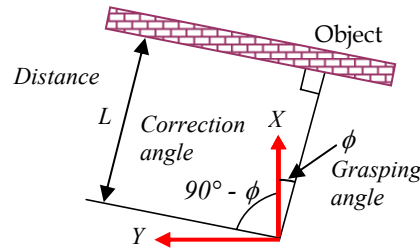
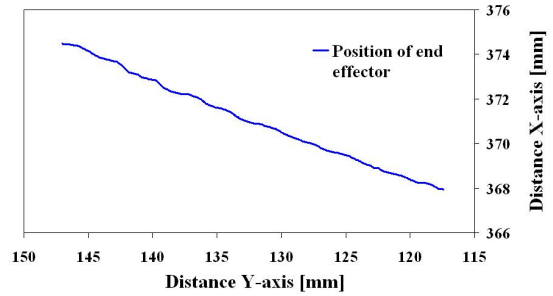


Fig. 7. Grasping motion (top). Graph of end-effector position in grasping front wall (middle). Robot orientation after grasping process (bottom).

In this research we have proposed a navigation method based on contact interaction for the humanoid robot to recognize its surroundings and define self-localization by touching and grasping object's surface [14]. Figure 6 shows motion planning in this research. All motions are derived by previously explained formulations of trajectory generation. Grasping of humanoid robot arm is a process in which the robot keeps its arm in contact with the wall's surface while performing a rubbing-like motion. The robot arms are equipped with force sensor as end-effector for force control. Figure 7 (top) shows photograph of the robot's arm during grasping on object surface. During grasping process, position data of the end-effector are defined, which described the object's surface orientation.

Based on the object's orientation, relative relations of distance and angle between the robot

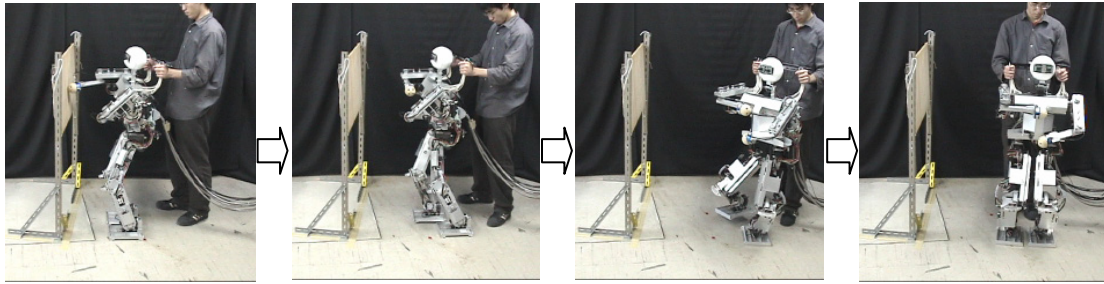


Fig. 8. Photographs of grasping front wall and correction of robot's locomotion direction experiment.

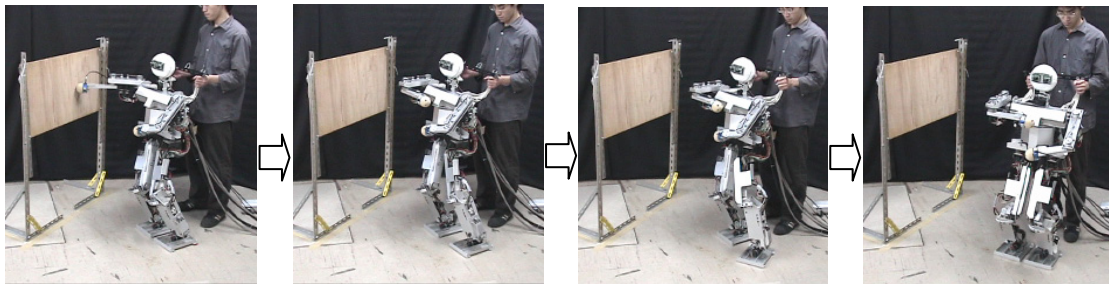


Fig. 9. Photographs of grasping side wall and correction of robot's locomotion direction experiment.

and the wall are obtained. The robot then responds to its surroundings by performing corrections to its orientation and locomotion direction. Basically, the application of sensors is necessary for a humanoid robot to recognize its surroundings. In this research, six-axis force sensors were attached to both arms as end-effectors that directly touch and grasp objects to provide force data that are subsequently converted to position data by the robot's control system.

The grasping process in the proposed navigation method is classified into two situations: grasping the front object and grasping the side object. For example, for grasping front object, the end-effector position data are plotted in graph as shown in Fig. 7 (middle), which described the object surface orientation that positioned at the robot's front. The end-effector data obtained during grasping process are calculated with the least-square method to define the wall orientation. Based on the object's orientation obtained in grasping process, relative relation of humanoid robot's position and angle are defined, like shown in geometrical analysis in Fig. 7 (bottom), where ϕ is grasping angle, and $90^\circ - \phi$ is a correction angle. Meanwhile L is the shortest distance from the humanoid robot to the object.

Humanoid robot correcting its orientation and locomotion direction based on the grasping result. This motion is important to avoid collision with any object especially wall during operation in human's environment. The algorithm of correction is consists of two: Correction of distance and correction of angle. In grasping front object, position of the object facing the robot creates possibility of collision during correction of the robot's orientation. Therefore, correction of robot's distance was simply

performed by generating trajectory for legs to walk to backwards direction.

In grasping side object, correction of distance involves trajectory generation of legs to walk side-step away from the object. However, if the grasping angle ϕ is $0 < \phi \leq 45^\circ$, it is still possible for the robot to collide with the object. In this case, the robot will walk one step to backward direction, before proceed to walk side-step. Eventually, if the grasping angle ϕ is $45^\circ < \phi \leq 90^\circ$, the robot will continue to correct its position by walking side-step away from the object. Correction of the robot's angles is performed by changing the robot orientation to $90^\circ - \phi$, so that the final robot's orientation is parallel with object's surface orientation. Correction of angle is focus on trajectory generation of the humanoid robot legs, especially for hip-joints.

Experiments with humanoid robot *Bonten-Maru II* were conducted to evaluate the performance of the proposed navigation method. Figures 8 and 9 show photographs of humanoid robot performing navigation experiments when objects are located at the robot's front and right-side area, respectively. The object in this experiment is a flat surface wall made from wood. After grasping process finished, the robot performed correction process of its orientation and locomotion direction. The robot's orientation after correction process is about parallel with the object's surface orientation. These experimental results indicated that the humanoid robot smoothly recognized the wall orientation and performed correction of locomotion direction by generating suitable leg trajectories. This will help humanoid robot to operate in dark area, and assist visual-based navigation.

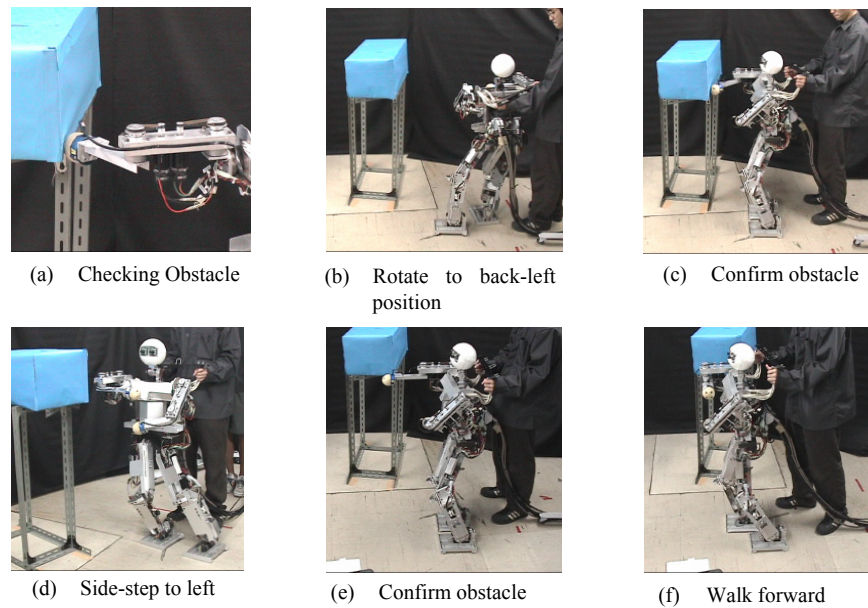


Fig. 10. Photographs of humanoid robot motions during avoiding high obstacle.

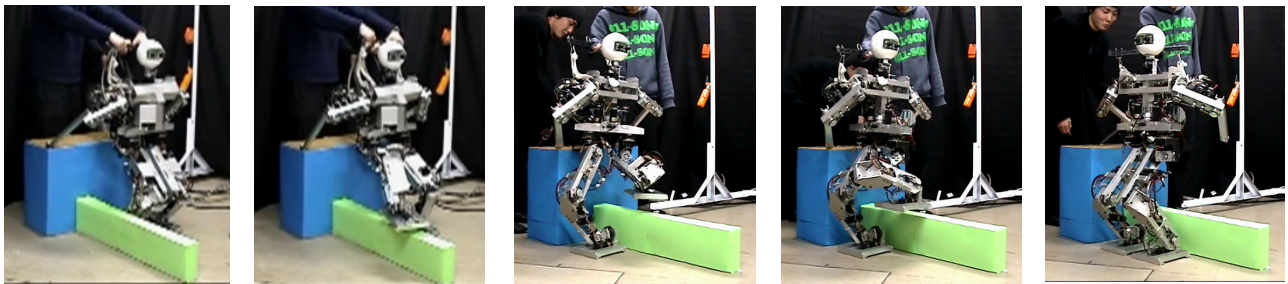


Fig. 11. Photographs of humanoid robot motions during avoiding low obstacle.

5 Motions of Obstacle Avoidance

In humanoid robots to effectively operate and collaborate with humans in real environments, the abilities to recognize and avoid obstacles are inevitably important. In this research, we proposed obstacle avoidance method, which is developed in conjunction with the proposed navigation explained in previous section.

5.1 Avoiding high obstacle

In avoiding high obstacle, the obstacle height is about the same height of the *Bonten-Maru II*. The concept of the obstacle-avoidance algorithm is based on trajectory generation of the humanoid robot's legs, with reference to the grasping results [15]. Leg positions are decided by interpolation using polynomial equations, and each joint position is given via angle data from calculation of the inverse kinematics needed to move the legs to the desired positions.

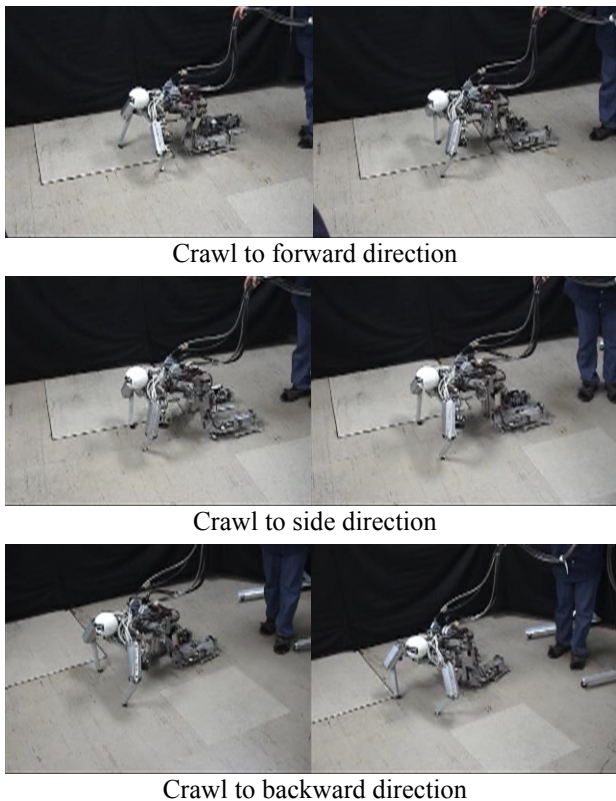
Obstacle avoidance is performed after correcting the robot's distance to the wall, before proceeding to the correct angle. As shown in Fig. 10, while checking the obstacle to the left, the left arm will search for and detect any obstacle that exists within the correction angle's area and up to the arm's

maximum length in order to instruct the robot's system either to proceed with the correction or to proceed with the next process of obstacle avoidance. If an obstacle is detected, the robot will rotate to the back-left position, changing its orientation to face the obstacle. The robot will then continuously recheck the existence of the obstacle by performing the "confirm obstacle" process. If no obstacle is detected, the robot will walk forward. However, if an obstacle was detected, instead of walking to forward direction, the robot will walk side-step towards its left side direction, and repeat again the confirmation process until no obstacle is detected. Then it will walks forward and complete the obstacle avoidance process.

5.2 Avoiding low obstacle

In avoiding low obstacle, the obstacle height is about the height from *Bonten-Maru II*'s foot to knee. The robot performs motion to hop over the obstacle with the help of both arms [16]. This motion is very critical especially for joints at hip and legs.

In this motion, the robot may detect the obstacle by visual sensors at the eyes, or range sensors at the bottom of its feet. Figure 11 shows demonstration of the humanoid robot stepping over a low obstacle.



Crawl to forward direction

Crawl to side direction

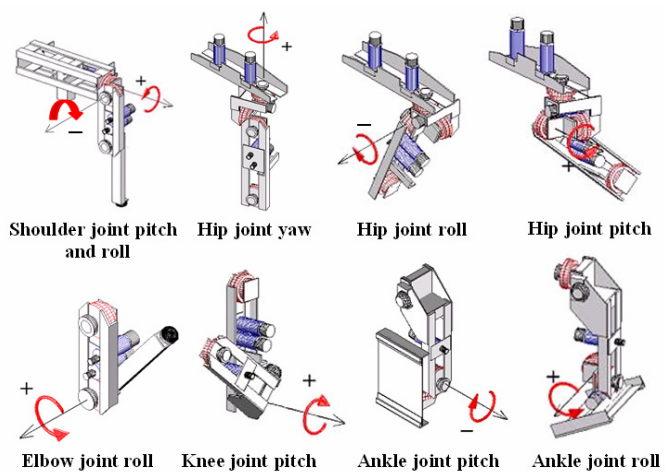
Crawl to backward direction

Fig. 12. Crawling motions of humanoid robot *Bonten-Maru II*.

6 Motions of Crawling

The ability to crawl on floor is developed and demonstrated with humanoid robot *Bonten-Maru II* as shown in Fig. 12 for application in hazardous site [17]. This motion considers the humanoid's joint structure design, joint rotation range and analysis of centre of gravity. In humanoid robot design, joint rotation angle are decided from consideration of elements such as correlation with human joint rotation angles, position of body parts, and body structure design. These elements lead to mobility and flexibility of humanoids' manipulators to attain complicated trajectories. Motion planning was designed considering joint rotation range in the robot's body to provide manipulability and flexibility to perform human-like motions, in addition to provide safety for the humanoid robot during locomotion.

Figure 13 shows joint structure of humanoid robot *Bonten-Maru II*'s arm and leg. Refer to Table 1, for example, the yaw component of the hip joint of both legs is rotated open wide until 90 degrees in the outer rotation direction and 60 degrees in the inner direction. Also for hip-joint-roll, the angle is 90 degrees in the outer rotation direction and only 22 degrees in the inner rotation. These angles provide an advantage to the humanoid robot in attaining difficult motion, as well protecting body

Fig. 10. Joint structure and rotation direction of *Bonten-Maru II*'s arm and leg.

parts from colliding with each other. For ankle joints (pitch and roll), the joint rotation range is designed to be wider than humans' in the outer rotation direction for the pitch and in the inner direction for roll, as shown in Fig. 13. The purpose is to compensate for the flexibility of shin muscles and the functions of toe joints in humans that not available in a humanoid's body structure. This is useful for performing difficult motion, especially crawling motion which can be applied in hazardous location.

7 Conclusions

In this research, we developed a basic motion in a biped humanoid robot *Bonten-Maru II* with the aim to contribute in human-robot interaction researches. We present experimental results of humanoid robot *Bonten-Maru II* to attain human-like motion. We managed to demonstrate a basic navigation method based on contact-interaction where humanoid robot used its arm to grasp wall and defined self-localization, then continuously correcting its position and locomotion direction, and avoiding obstacle. Related with obstacle avoidance, we have demonstrated methods to avoiding high and low obstacle. In this report also, we presented crawling motion of the robot to crawl on floor in numerous directions.

The experimental results reveal good performance of the robot when performing human-like motions in the proposed navigation method, obstacle avoidance, and crawling motions. In the experiments of contact-based navigation, autonomous motions of the robot's manipulators are managed to demonstrate. These satisfy the objective of this research to develop autonomous navigation system based on contact interaction to improve visual-based navigation. This will help the robot to

operate effectively and safely in built-for-human's environments. The results presented in this report provide basic foundations for further research and development of humanoid robots performing human-like motion. It is anticipated that using this fundamental research will help advance the evolution of humans and robots working together in real life. In addition, the proposed idea should contribute to better understanding of interactions between robots and its surroundings.

Future work will include further development of the contact-based humanoid robot navigation system project for real-time applications. To generate optimal gait energy in bipedal walk of the navigation tasks, we consider a real time generation of optimal gait by using Genetic Algorithms (GA).

8 Acknowledgement

Part of this research was supported by a fiscal 2006 grants from the Japan Ministry of Education, Culture, Sports, Science and Technology (Grant-in-Aid for Scientific Research in Exploratory Research, No. 18656079), and Grant-in-Research by Japan Society for the Promotion of Science (JSPS).

References:

- [1] K. Hirai, M. Hirose, Y. Haikawa and T. Takenaka, "The Development of Honda Humanoid Robot," in *Proc. of IEEE Int. Conference on Robotics and Automation*, 1998, pp. 1321-1326.
- [2] M. Vukobratovic, B. Borovac and K. Babkovic, "Contribution to the Study of Anthropomorphism of Humanoid Robots," *Humanoids Robotics J.*, Vol. 2, No.3, 2005, pp. 361-387.
- [3] H. Lim, Y. Yamamoto and A. Takanishi, "Control to Realize Human-Like walking of a Biped Humanoid Robot," in *Proc. IEEE Int. Conf. System, Man and Cybernetics*, Vol. 5, 2000, pp. 3271-3276.
- [4] R. Dillmann, "Teaching and Learning of Robot Tasks via Observation of Human Performance," *Robotics and Autonomous Systems J.*, Vol. 47, 2004, pp. 109-116.
- [5] J. Wang, T. Sheng, J. Wang and H. Ma, "System Overview of The Humanoid Robot Blackman," *WSEAS Transactions on Systems*, Vol. 4, Issue 7, July 2005, pp.1070-1075.
- [6] S. Kaneko, Y. Nasu, M. Yamano, K. Mitobe & G. Capi, "Online Remote Control of Humanoid Robot Using a Teleoperation System and User Interface," *WSEAS Transactions on Systems*, Vol. 4, Issue 5, May 2005, pp.561-568.
- [7] Y. Nasu, G. Capi, M. Yamano, "Development and Perspectives of a Humanoid Robot Project," in *Proc. of 7th Int. Pacific Conference on Manufacturing and Management (PCMM)*, Vol.1, 2002, pp. 240-245.
- [8] Y. Hanafiah, M. Yamano, Y. Nasu and M. Ohka, "Design of a 21-DOF Humanoid Robot to Attain Flexibility in Human-Like Motion," in *Proc. 15th IEEE Int. Symposium on Robot and Human Interactive Communication (ROMAN2006)*, 2006, pp. 202-207.
- [9] S. Kajita, T. Nagasaki, K. Kaneko, K. Yokoi, & K. Tanie, "A Running Controller of Humanoid Biped HRP-2LR". In *Proceeding of International Conference on Robotics and Automation (ICRA05)*, 2005, pp. 618-624.
- [10] R. Koker "Reliability-Based Approach to the Inverse Kinematics Solution of Robots Using Elman's Network", *Journal of Engineering Application of Artificial Intelligence*, Vol. 18, No. 6, 2005, pp. 685-693.
- [11] Y. Hanafiah, M. Yamano, Y. Nasu and M. Ohka, "Trajectory Generation in Groping Locomotion of a 21-DOF Humanoid Robot," in *CDR Proc. 9th Int. Conf. on Mechatronics Technology*, 2005, ICMT-54.
- [12] J. Denavit, & S. Hartenberg, "A Kinematics Notation for Lower-Pair Mechanisms Based Upon Matrices", *Journal of Applied Mechanics*, Vol. 77, 1995, pp. 215-22.
- [13] A. Konno, "Development of an Anthropomorphic Multi-Finger Hand and Experiment on Grasping Unknown Object by Groping," *Transaction of the JSME*, Vol.65, No. 638, 1999, pp 4070-4075.
- [14] Y. Hanafiah, M. Yamano, M. Ohka, and Y. Nasu, "Development of a Contact Interaction-Based Navigation Strategy for a Biped Humanoid Robot," In *Proceedings of 2007 IEEE/RSJ International Conference on Intelligent Robots and Systems (IROS07)*, 2007, pp. 4241-4246.
- [15] Y. Hanafiah, M. Yamano, Y. Nasu, K. Mitobe, M. Ohka, "Obstacle Avoidance in Groping Locomotion of a Humanoid Robot", *Int. Journal of Advanced Robotic Systems*, Vol. 2 No. 3, 2005, pp. 251-258.
- [16] M. Yamano, Y. Nasu, R. Sato, K. Mitobe, Y. Hanafiah, "Motion Planning of a Biped Humanoid Robot that Steps Over an Obstacle Using its Hands," in *CD-R Proc. 9th Int. Conf. on Mechatronics Tech.*, 2005, ICMT-151.
- [17] M. Yamano, Y. Nasu, S. Kaneko, R. Sato and K. Mitobe, "Creeping Motion of a Humanoid Robot on its Hands and Knees," in *CD-R Proc. FIRA Robot World Congress 2003*, 2003.